AD-A156 735 ANALYSIS OF EDGE DETECTION ALGORITHMS ON DIAL (DIGITAL IMAGE ANALYSIS LABORATORY)(U) ARMY ENGINEER TOPOGRAPHIC LABS FORT BELVOIR VA J M BROWN JAN 85 ETL-0371 1/1

UNCLASSIFIED F/G 12/1 NL

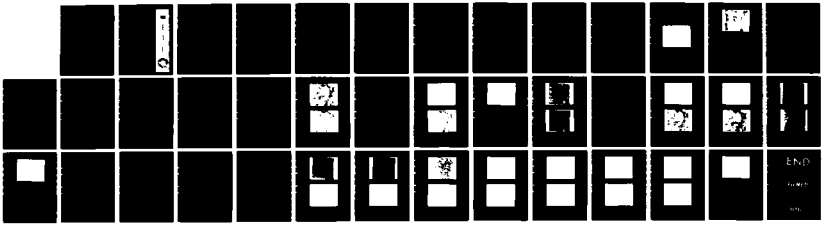

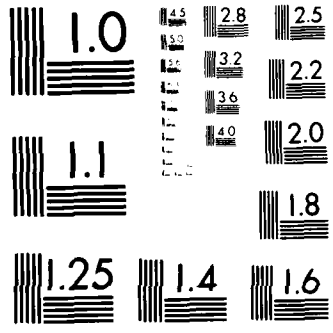

MICROCOPY RESOLUTION TEST CHART

ETL-0371

Analysis of edge detection algorithms on DIAL

Jane M. Brown

January 1985

US ARMY CORPS OF ENGINEERS
ENGINEER TOPOGRAPHIC LABORATORIES
FORT BELVOIR, VIRGINIA 22060-5546

E T L

Destroy this report when no longer needed.
Do not return it to the originator.

The findings in this report are not to be construed as an official Department of the Army position unless so designated by other authorized documents.

The citation in this report of trade names of commercially available products does not constitute official enforcement or approval of the use of such products.

REPORT DOCUMENTATION PAGE

READ INSTRUCTIONS BEFORE COMPLETING FORM

1. REPORT NUMBER ETL - 0371	2. GOVT ACCESSION NO. AD-A156735 / 3. RECIPIENT'S CATALOG NUMBER
4. TITLE (and Subtitle) ANALYSIS OF EDGE DETECTION ALGORITHMS ON DIAL	5. TYPE OF REPORT & PERIOD COVERED Research Note 6. PERFORMING ORG. REPORT NUMBER
7. AUTHOR(s) Jane M. Brown	8. CONTRACT OR GRANT NUMBER(s)
9. PERFORMING ORGANIZATION NAME AND ADDRESS U.S. Army Engineer Topographic Laboratories Fort Belvoir, VA 22060-5546	10. PROGRAM ELEMENT, PROJECT, TASK AREA & WORK UNIT NUMBERS 4A762707A855,B,0026
11. CONTROLLING OFFICE NAME AND ADDRESS U.S. Army Engineer Topographic Laboratories Fort Belvoir, VA 22060-5546	12. REPORT DATE January 1985 13. NUMBER OF PAGES 37
14. MONITORING AGENCY NAME & ADDRESS(if different from Controlling Office)	15. SECURITY CLASS. (of this report) Unclassified 15a. DECLASSIFICATION/DOWNGRADING SCHEDULE

16. DISTRIBUTION STATEMENT (of this Report)

Approved for public release; distribution is unlimited.

17. DISTRIBUTION STATEMENT (of the abstract entered in Block 20, if different from Report)

18. SUPPLEMENTARY NOTES

19. KEY WORDS (Continue on reverse side if necessary and identify by block number)

Feature Extraction	Zero-Crossing (2nd Order Differential) Operator
Edge Detection	Sobel
Nonlinear Edge Masks	Marr Edge Detector
Directional Edge Masks	Prewitt Edge Masks
Relaxation	Kirsch Edge Masks

20. ABSTRACT (Continue on reverse side if necessary and identify by block number)

A study was conducted to determine whether selected edge-finding algorithms could be used in a semiautomated feature extraction system to find lineal features such as roads and boundaries. This research note analyzes and compares selected edge-finding algorithms, and comments on their integration with other feature classification algorithms.

PREFACE

The work covered by this research note was conducted by the U.S. Army Engineer Topographic Laboratories (ETL), Fort Belvoir, Virginia. It is part of an effort carried out on feature extraction under DA Project 4A762707A855, Task B, Work Unit 0026, "Topographic Mapping Techniques."

Studies were conducted by Ms. Jane M. Brown under the guidance of Mr. Michael A. Crombie and supervision of Mr. Dale Howell, Chief, Information Sciences Division, and Mr. Lawrence A. Gambino, Director, Computer Sciences Laboratory.

COL Edward K. Wintz, CE, was Commander and Director and Mr. Walter E. Boge was Technical Director of the Engineer Topographic Laboratories during the report preparation.

CONTENTS

ILLUSTRATIONS

ANALYSIS OF EDGE DETECTION ALGORITHMS ON DIAL

INTRODUCTION

As part of an effort to deliver to the Defense Mapping Agency (DMA) in FY85 a semiautomated feature extraction system, the Engineer Topographic Laboratories (ETL) is conducting a feature extraction study. One of the objectives of this study is to determine whether selected edge-finding algorithms can be used to find such lineal features as roads and boundaries.

PURPOSE

The purpose of this ~~research note~~ is to report on progress to date on an analysis of several edge-detection algorithms that exist on ETL's Digital Image Analysis Laboratory (DIAL) image-processing facility. In addition to evaluating the algorithms, this study investigated the possibilities of integrating the algorithms' resultant edges with other feature classification algorithms. Three fundamental edge-detection methods were compared:

1. A nonlinear edge-enhancement operator.
2. A directional edge operator.
3. An extraction of the zero-crossings from filtering an image with the Laplacian of a symmetric Gaussian function.

DIAL FACILITY

DIAL is an interactive image-processing facility consisting of a host computer (CYBER 170-730), an associative array processor (STARAN), and a real-time processing and display subsystem. Several of the edge-detection program modules (PM's) require computationally bound mathematical operations that would be too laborious and time-consuming on a sequential machine such as the CYBER 170-730. In order that the computations be done as efficiently and as expediently as possible, the services of the array processor, STARAN, which processes data in parallel rather than sequentially, were engaged. The STARAN in conjunction with the CYBER and the DIAL system enables an operator to produce interactive tests in a timely fashion. The DIAL facility is also interfaced with a Dunn camera system that photographs a digital image on the DIAL display screen. This camera was used to take the pictures included in

this report, and although this camera does not produce the sharpest representation of the display image, its photographs are an improvement over any other process we have used thus far. A more detailed overview of the DIAL facility is presented by Norvelle.[1]

TEST IMAGES

In order to compare the results of the various algorithms, all tests were performed on the same scenes, CBP54A (figure 1) and its stereomate CBP56A (figure 2), both of which are subsets of a panchromatic image taken near the U.S.-Canadian border. Each scene is a 512 by 512, 8-bit image.

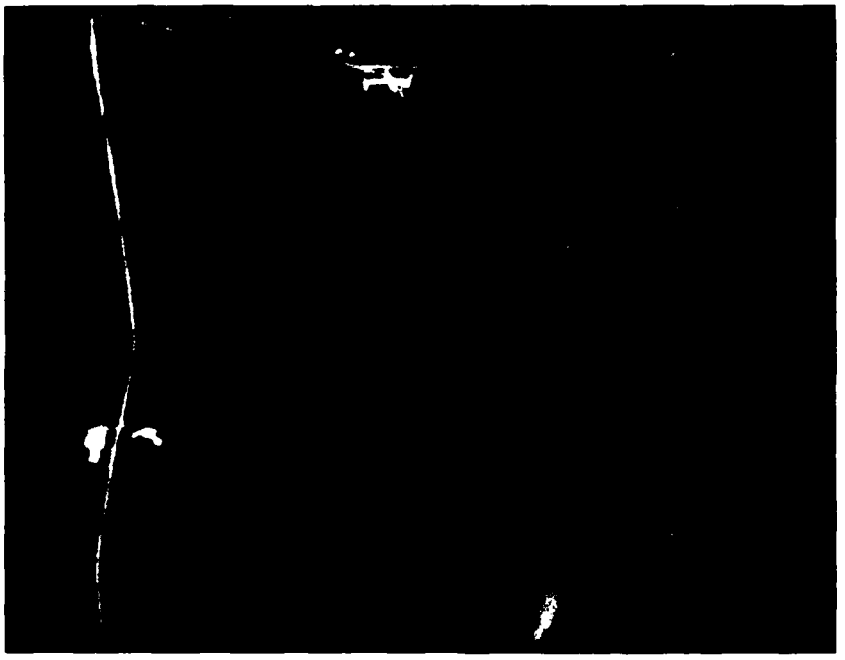

Figure 1. Scene CBP54A.

[1]F. R. Norvelle, Interactive Digital Correlation Techniques for Automatic Compilation of Elevation Data, U.S. Army Engineer Topographic Laboratories, Fort Belvoir, Va., ETL-0272, October 1981, AD-A109 145.

Figure 2. Scene CBP56A (Stereomate of CBP54A).

THE ALGORITHMS

There were three basic types of edge operators tested in this study. The first was a nonlinear edge-enhancement operator; the second was a directional-edge operator; and the third employed a second-difference operator and then determined the zero-crossings of the response.

Nonlinear - The Sobel operator was selected from several nonlinear edge-enhancement operators for comparison with other types of operators; it utilizes a 3 by 3 window of information around the pixel rather than only the neighbors to the right and below as is the case in a 2 by 2 operator. The Sobel operator[2] computes a new pixel gray value (G) in the following manner:

$$G = \sqrt{X^2 + Y^2}$$

where

---

[2]W. K. Pratt, Digital Image Processing, a Wiley-Interscience Publication, John Wiley & Sons, New York, 1978.

$$X = (A_2 + 2A_3 + A_4) - (A_0 + 2A_7 + A_6)$$

and $$Y = (A_0 + 2A_1 + A_2) - (A_6 + 2A_5 + A_4)$$

and A_i, $i = 0, 7$ are located around the pixel P:

A_0	A_1	A_2
A_7	P	A_3
A_6	A_5	A_4

Computations for the Sobel PM are performed by the CYBER 170-730 computer.

Directional Edge - The directional-edge operator tested under this study is a relaxation technique[3] whereby a set of directional-edge masks are utilized to generate a set of likelihood values that an edge exists in one of eight directions. These likelihood values are then enhanced by a relaxation process that iteratively updates the likelihood values in an attempt to reliably define edge definitions.

Because of computational limitations, only edge masks of size 3 by 3 and 5 by 5 were used in this study. The 3 by 3 set of masks in figure 3 is typical of directional-edge masks.

NE
$$\begin{bmatrix} 1 & 1 & 1 \\ -1 & -2 & 1 \\ -1 & -1 & 1 \end{bmatrix}$$
SW
$$\begin{bmatrix} 1 & -1 & -1 \\ 1 & -2 & -1 \\ 1 & 1 & 1 \end{bmatrix}$$

N
$$\begin{bmatrix} 1 & 1 & 1 \\ 1 & -2 & 1 \\ -1 & -1 & -1 \end{bmatrix}$$
S
$$\begin{bmatrix} -1 & -1 & -1 \\ 1 & -2 & 1 \\ 1 & 1 & 1 \end{bmatrix}$$

NW
$$\begin{bmatrix} 1 & 1 & 1 \\ 1 & -2 & -1 \\ 1 & -1 & -1 \end{bmatrix}$$
SE
$$\begin{bmatrix} -1 & -1 & 1 \\ -1 & -2 & 1 \\ 1 & 1 & 1 \end{bmatrix}$$

W
$$\begin{bmatrix} 1 & 1 & -1 \\ 1 & -2 & -1 \\ 1 & 1 & -1 \end{bmatrix}$$
E
$$\begin{bmatrix} -1 & 1 & 1 \\ -1 & -2 & 1 \\ -1 & 1 & 1 \end{bmatrix}$$

Figure 3. Compass gradient Prewitt edge masks.

[3] R. A. Lott, R.O. Faiss, S.G. Stadelman, STARAN Image Processing, Final Technical Report, U.S. Army Engineer Topographic Laboratories, Fort Belvoir, Va., ETL 0243, October 1980, AD-A091 928.

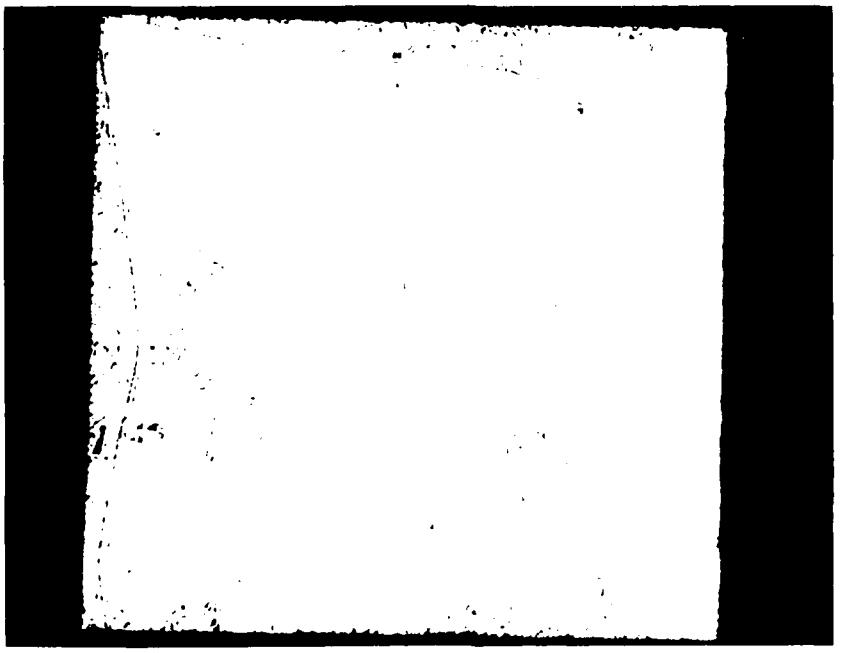

Figure 20. Zero-crossings of 7 by 7 Marr window with $\sigma = 1$ convolved with CBP54A.

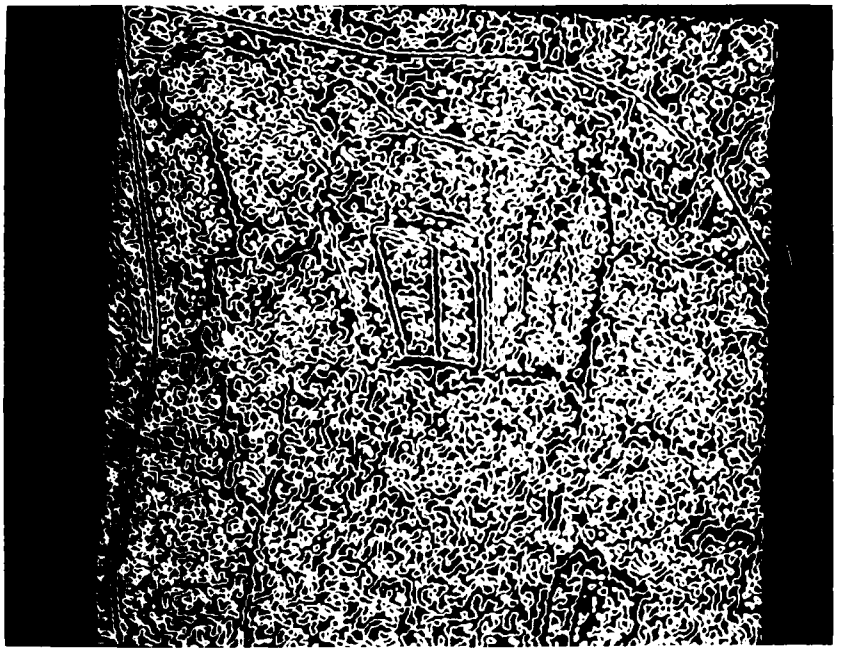

Figure 21. Zero-crossings of 15 by 15 Marr window with $\sigma = 2$ convolved with CBP54A.

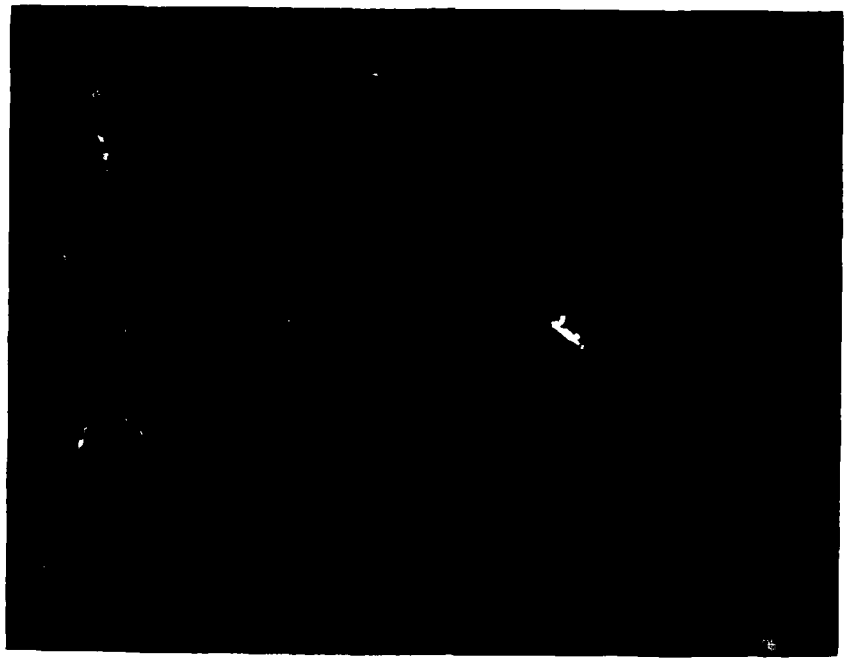

Figure 18. Relaxation on CBP54A using Kirsch directional masks, 1st iteration.

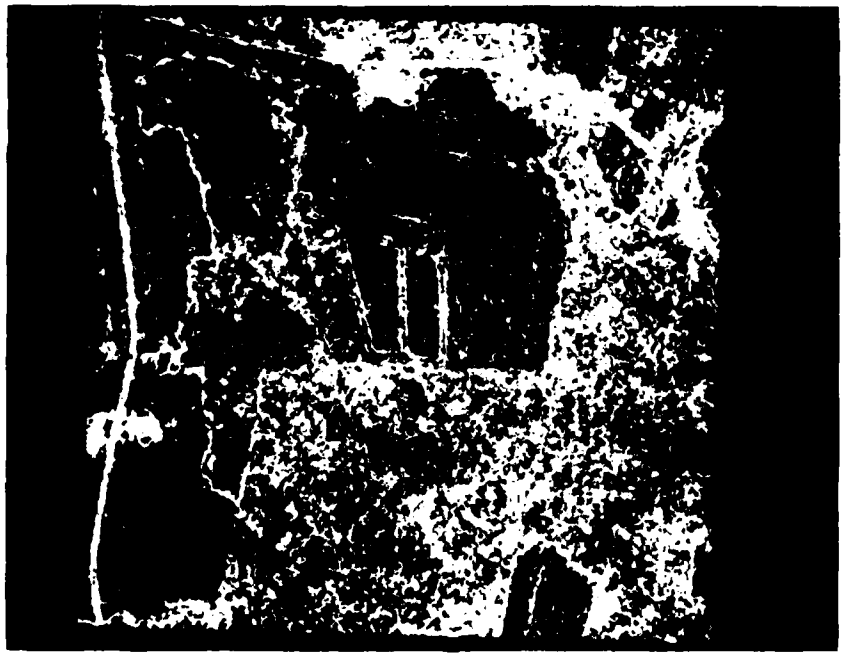

Figure 19. Relaxation on CBP54A using Kirsch directional masks, 3rd iteration.

Figure 16. Relaxation on CBP54A using Prewitt directional masks, 1st iteration.

Figure 17. Relaxation on CBP54A using Prewitt directional masks, 3rd iteration.

When used in the relaxation algorithm, results of four convolutions (the N, NW, W, and NE masks) are merged to form a set of probabilities that are "relaxed" and iterated while using the directional probabilities of the pixel's neighbors. Figure 16 is the first iteration result of the convolution and relaxation of Prewitt edge masks with CBP54A, while figure 17 shows the third iteration. Figures 18 and 19 are the first and third iterations of the same technique used on the Kirsch set of directional masks.

A 5 by 5 set of directional masks by Barnard was also tried with the relaxation technique but produced results no better than the Kirsch masks and involved almost three times the number of computations. In order to use the results of the relaxation algorithm in a feature extraction scheme, the results would again have to be segmented into a binary representation to define an "edge/no edge" existence.

Figure 21 is the result of the Marr Window in figure 7 convolved with the same image.

Figure 22 depicts the results of a Marr Window with $\sigma = 3$ convolved with CBP54A.

In addition to road and field edges, the Marr zero-crossings algorithm was tested on a drainage pattern that is a subscene of a Phoenix test model. Results of this series of tests are shown in appendix A.

DISCUSSION

This discussion will be limited to the quality of the results, not the amount of time elapsed in the computations. Time discussions are neither appropriate nor fair because some processes utilize a parallel processor for computations while others use sequential processors. Then, too, the DIAL configuration utilizes a conglomeration of computer hardware, and each edge-detection algorithm uses its own combination to achieve the final results.

Sobel - The Sobel operator performed admirably in delineating edges and missed very few edges. It was difficult, however, to extract a binary image by thresholding and still keep the major edges intact. Clutter removal tended to break up several of these prominent edges.

Directional Edge - Although the relaxation technique produced poor results with the first iteration, the third iteration did only slightly poorer than the Sobel operator. The Prewitt set of masks did not perform as well as the Kirsch set of masks, the latter giving finer detail along edges.

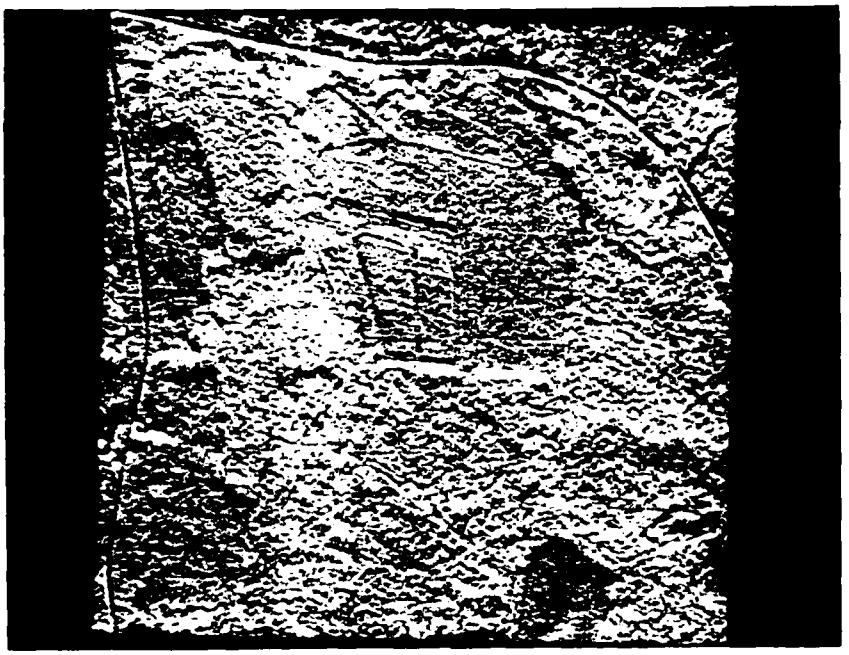

Figure 14. CBP54A convolved with Prewitt's north gradient mask.

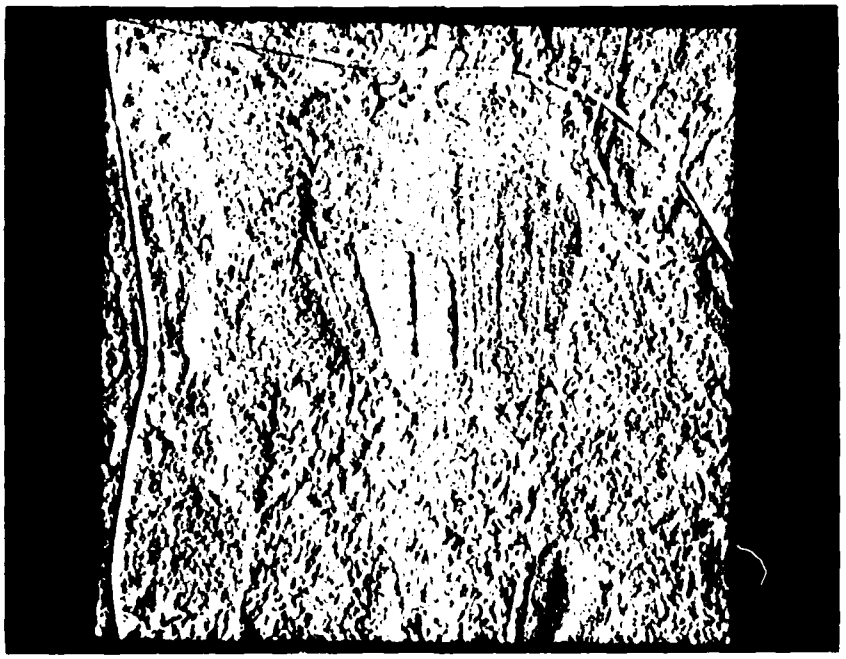

Figure 15. CBP54A convolved with Prewitt's west gradient mask.

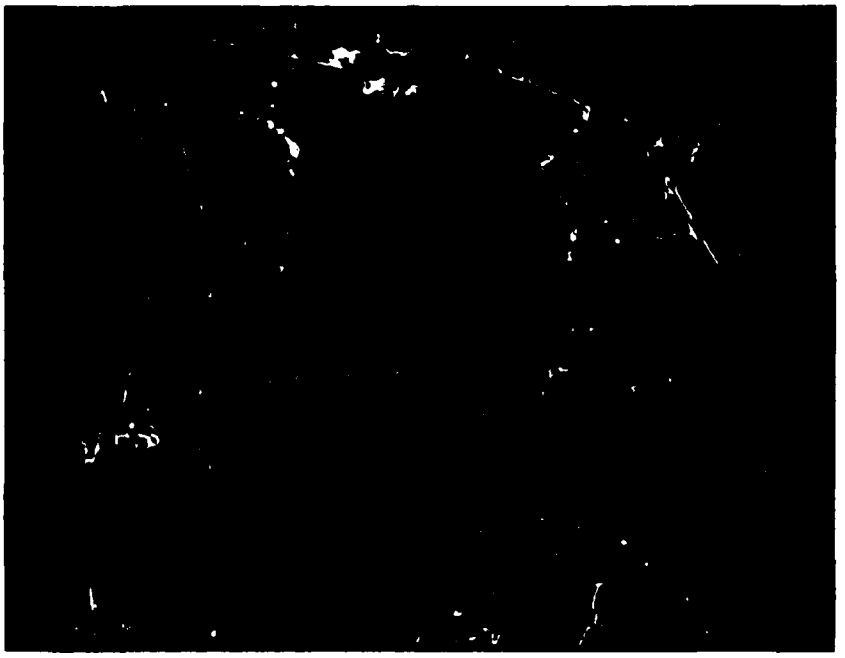

Figure 13. Sobel image CBSOB thresholded at gray shade 235.

Directional Relaxation - As previously stated, the relaxation process involves a set of four directional masks. The set included above is attributed to Prewitt.[7] Two other sets have been studied here: the Kirsch[8] directional masks and a set of 5 by 5 masks by Barnard.[9] Figure 14 shows a convolution of the Prewitt north gradient mask with CBP54A and figure 15 is the convolution of the west gradient mask with the same image.

---

[7]H.C. Andrews, Interactive Real-Time Adaptive Nonlinear Convolution, Image Processing Application Note, University of Southern California, Los Angeles, CA 90007, no date.

[8]Ibid.

[9]S. Barnard, Application of Image Understanding to Cartography, SRI International report 8718, prepared for DMAAC/LOP, March 1981.

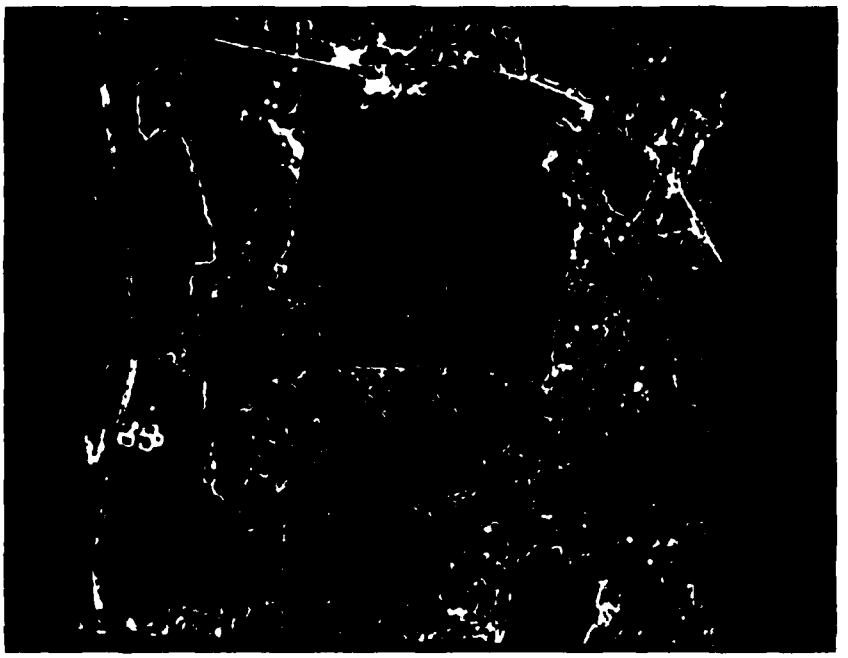

Figure 11. Sobel image CBSOB thresholded at gray shade 200.

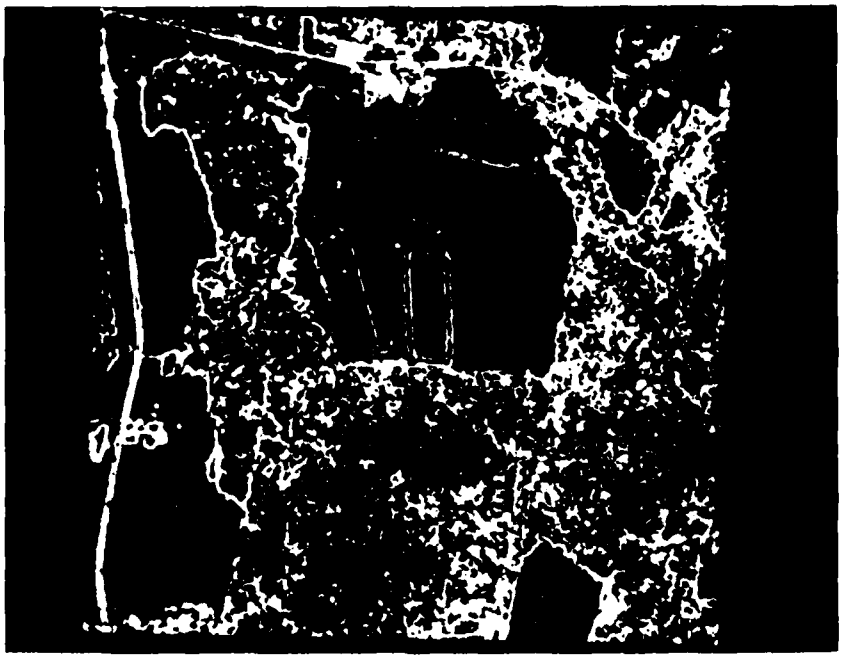

Figure 12. Sobel image CBSOB thresholded at gray shade 135.

Marr results depicted in this report were generated by a convolution of the Marr windows with the image in the frequency domain using the FOURIER PM written by Mr. Robert Pazak of ETL. This PM was modified to handle filters up to size 49 by 49 on images of size 512 by 512 and utilizes the CYBER.

RESULTS

It is rather difficult to measure how well an edge-detection algorithm performs since the results are all visual and there are no statistics generated nor any standards with which to compare the results. Too, the laborious task of rectification and registration of the images was not undertaken, so it was not possible to compare extracted edges to a map sheet.

Because we do not intend to use the results of edge-detection algorithm extractions as a final product, we are not concerned by the generation of noise and clutter. Those can be removed through a clean-up process on DIAL called RASTER.[6] In RASTER, edges can be thickened to join broken line segments or thinned to the center line of line widths several pixels thick, and clutter or noise can be eliminated. Future additions to RASTER will include a directional line-growing technique and area-fill for use with the Marr algorithm. We are concerned, however, with how well the algorithm depicted the presence of edges, if it generated non-existing edges or ignored edges that do exist. Algorithm results also have to be put into some useable form (binary preferred) in order to use them in combination with other feature-extraction results. Results of the edge-extraction algorithms are herewith presented.

Sobel. The Sobel operator yields an 8-bit image representation upon completion. The results are shown in figure 9, CBSOB1. Figure 10, CBSOB1S, shows the results of the Sobel operation on the stereomate CBP56A. Note that some edges, e.g., on field in center of photo, are not delineated as well as in figure 9. Several lines of data in the upper portion of CBSOB1S are the results of scratches in the original digitized transparency and should be ignored. The Sobel results were then thresholded in order to utilize them in conjunction with other feature extraction results. Figures 11, 12, and 13 show figure 9, a 256 gray shade representation, thresholded at gray shades 200, 135, and 235 respectively.

---

[6] N. Friend, Analysis of Interactive Image Cleansing via RASTER-Processing Techniques, U.S. Army Engineer Topographic Laboratories, Fort Belvoir, Va., ETL-0347, November 1983, AD-A141 772.

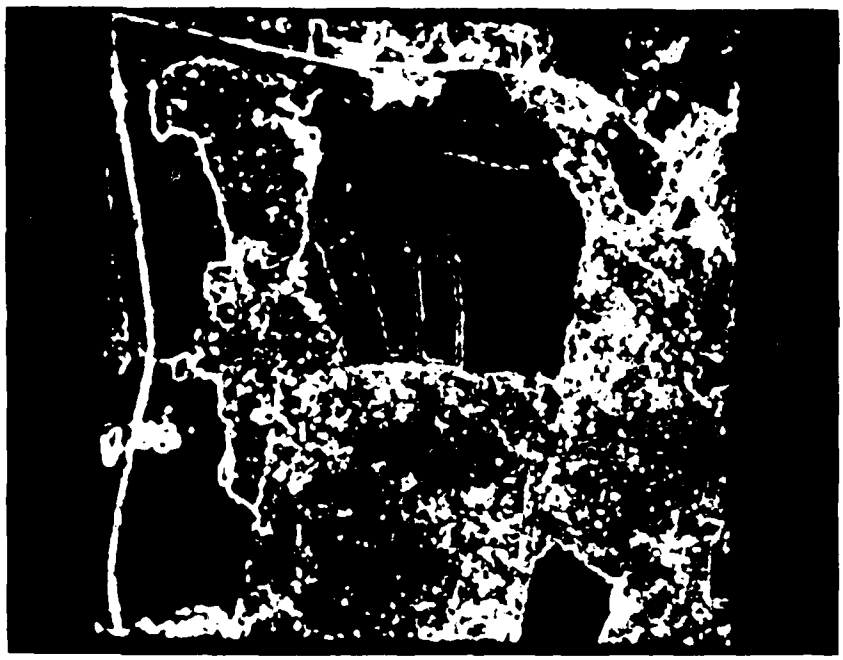

Figure 9. CBSOB1 - Sobel operation on CBP54A.

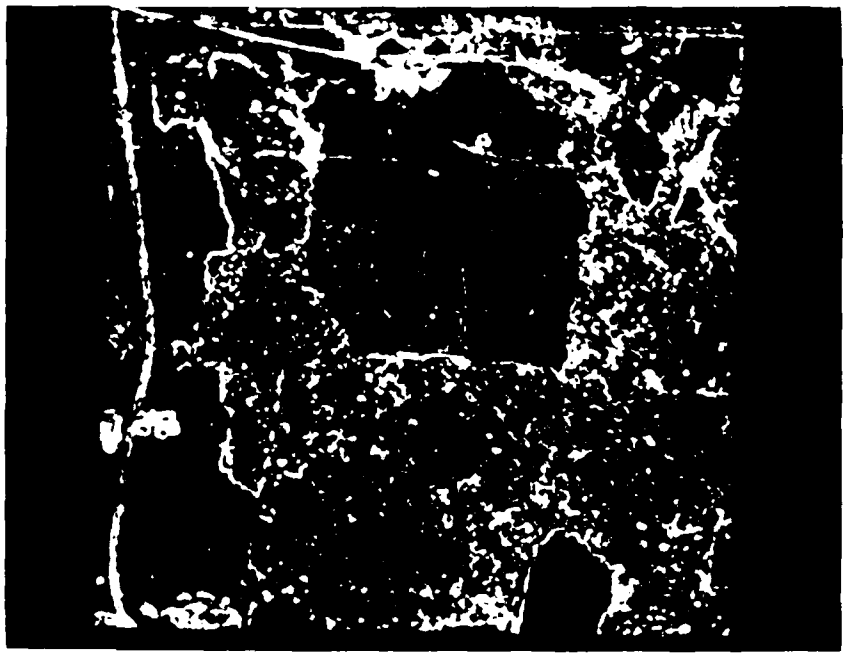

Figure 10. CBSOB1S - Sobel operation on CBP56A.

	1	2	3	4	5	6	7	8	9	10	11	12	13	14
1	-.00	-.00	-.00	-.00	-.00	-.00	-.00	-.00	-.00	-.01	-.01	-.01	-.01	-.01
2	-.00	-.00	-.00	-.00	-.00	-.00	-.00	-.01	-.01	-.02	-.03	-.03	-.04	-.04
3	-.00	-.00	-.00	-.00	-.00	-.01	-.01	-.02	-.04	-.06	-.08	-.10	-.12	-.12
4	-.00	-.00	-.00	-.00	-.01	-.02	-.03	-.06	-.10	-.16	-.21	-.27	-.30	-.32
5	-.00	-.00	-.00	-.01	-.02	-.04	-.08	-.15	-.24	-.36	-.49	-.60	-.67	-.70
6	-.00	-.00	-.01	-.02	-.04	-.09	-.18	-.32	-.51	-.73	-.95	-1.14	-1.27	-1.31
7	-.00	-.00	-.01	-.03	-.08	-.18	-.35	-.60	-.92	-1.27	-1.59	-1.84	-1.99	-2.04
8	-.00	-.01	-.02	-.06	-.15	-.32	-.60	-.99	-1.45	-1.89	-2.22	-2.38	-2.43	-2.44
9	-.00	-.01	-.04	-.10	-.24	-.51	-.92	-1.45	-1.99	-2.36	-2.42	-2.20	-1.89	-1.75
10	-.01	-.02	-.06	-.16	-.36	-.73	-1.27	-1.89	-2.36	-2.37	-1.75	-.66	.39	.82
11	-.01	-.03	-.08	-.21	-.49	-.95	-1.59	-2.22	-2.42	-1.75	0.00	2.43	4.59	5.46
12	-.01	-.03	-.10	-.27	-.60	-1.14	-1.84	-2.38	-2.20	-.66	2.43	6.41	9.85	11.21
13	-.01	-.04	-.12	-.30	-.67	-1.27	-1.99	-2.43	-1.89	.39	4.59	9.85	14.32	16.08
14	-.01	-.04	-.12	-.32	-.70	-1.31	-2.04	-2.44	-1.75	.82	5.46	11.21	16.08	18.00

Figure 8. Upper left quadrant of 27 by 27 Marr window for $\sigma = 3$.

	1	2	3	4	5	6	7
1	-.00	-.02	-.05	-.08	-.05	-.02	-.00
2	-.02	-.11	-.25	-.27	-.25	-.11	-.02
3	-.05	-.25	0.00	.61	0.00	-.25	-.05
4	-.08	-.27	.61	2.00	.61	-.27	-.08
5	-.05	-.25	0.00	.61	0.00	-.25	-.05
6	-.02	-.11	-.25	-.27	-.25	-.11	-.02
7	-.00	-.02	-.05	-.08	-.05	-.02	-.00

Figure 6. Marr window for $\sigma = 1$.

x	1	2	3	4	5	6	7	8	9	10	11	12	13	14	15
1	-.00	-.00	-.01	-.02	-.04	-.06	-.08	-.09	-.08	-.06	-.04	-.02	-.01	-.00	-.00
2	-.00	-.01	-.03	-.07	-.13	-.22	-.28	-.31	-.28	-.22	-.13	-.07	-.03	-.01	-.00
3	-.01	-.03	-.08	-.20	-.37	-.56	-.70	-.75	-.70	-.56	-.37	-.20	-.08	-.03	-.01
4	-.02	-.07	-.20	-.44	-.75	-.99	-1.07	-1.08	-1.07	-.99	-.75	-.44	-.20	-.07	-.02
5	-.04	-.13	-.37	-.75	-1.05	-.98	-.57	-.32	-.57	-.98	-1.05	-.75	-.37	-.13	-.04
6	-.06	-.22	-.56	-.99	-.98	0.00	1.61	2.43	1.61	0.00	-.98	-.99	-.56	-.22	-.06
7	-.08	-.28	-.70	-1.07	-.57	1.61	4.67	6.18	4.67	1.61	-.57	-1.07	-.70	-.28	-.08
8	-.09	-.31	-.75	-1.08	-.32	2.43	6.18	8.00	6.18	2.43	-.32	-1.08	-.75	-.31	-.09
9	-.08	-.28	-.70	-1.07	-.57	1.61	4.67	6.18	4.67	1.61	-.57	-1.07	-.70	-.28	-.08
10	-.06	-.22	-.56	-.99	-.98	0.00	1.61	2.43	1.61	0.00	-.98	-.99	-.56	-.22	-.06
11	-.04	-.13	-.37	-.75	-1.05	-.98	-.57	-.32	-.57	-.98	-1.05	-.75	-.37	-.13	-.04
12	-.02	-.07	-.20	-.44	-.75	-.99	-1.07	-1.08	-1.07	-.99	-.75	-.44	-.20	-.07	-.02
13	-.01	-.03	-.08	-.20	-.37	-.56	-.70	-.75	-.70	-.56	-.37	-.20	-.08	-.03	-.01
14	-.00	-.01	-.03	-.07	-.13	-.22	-.28	-.31	-.28	-.22	-.13	-.07	-.03	-.01	-.00
15	-.00	-.00	-.01	-.02	-.04	-.06	-.08	-.09	-.08	-.06	-.04	-.02	-.01	-.00	-.00

Figure 7. Marr window for $\sigma = 2$.

derivative of the distribution peaks, i.e., wherever zero-crossings in the second derivative occur. The second derivative used in our study was derived from the Gaussian distribution in two dimensions:

$$G(r) = \frac{1}{2\pi\sigma^2} e^{-\frac{r^2}{2\sigma^2}}$$

where $r^2 = x^2 + y^2$

The second-order differential operator that Marr (and we) used was the Laplacian because it is orientation-independent, being able to detect uniform intensity changes running down the y-axis as well as along the x-axis. The Laplacian is defined as the sum of the second derivatives of a function with respect to its directions:

$$LP\ (x,y) = \frac{\partial^2 G}{\partial x^2} + \frac{\partial^2 G}{\partial y^2}$$

and after the appropriate substitutions are made:

$$LP(x,y) = \frac{G(r)}{\sigma^2}\left[\frac{x^2 + y^2}{\sigma^2} - 2\right]$$

This Laplacian is used to generate a filter window to be convolved with the image, using values of x and y to indicate the distance from the center of the filter. For example, for a window of size 7, the center filter element would be calculated using x=y=0, whereas filter element 1,1 would be calculated using x=y=-3. Note that since all x's and y's in LP (x,y) and G(r) are squared, all filter windows generated are symmmetric with respect to both axes. Another variable in the Laplacian formula is the spread parameter, which Marr utilized to deal with changes that occur at different scales. Marr's theory in dealing with more than one spread parameter was that if two or more filters with varying spread parameters produced results that agreed, then most likely the edges in the image were real (as owing to a change in reflectance, illumination, depth, or surface orientation). If the "edges" did not occur in more than one convolution, then most likely that "edge" was the result of noise. For a further discussion of Marr windowing techniques, see appendix A.

Figures 6, 7, and 8 are examples of Marr windows created using several spread parameters.

In the second step of the relaxation algorithm, the gray shade value of each pixel is replaced by the probability vector for that pixel, which is then enhanced by a relaxation process using the information of the probability vectors of four neighboring pixels. See figure 5.

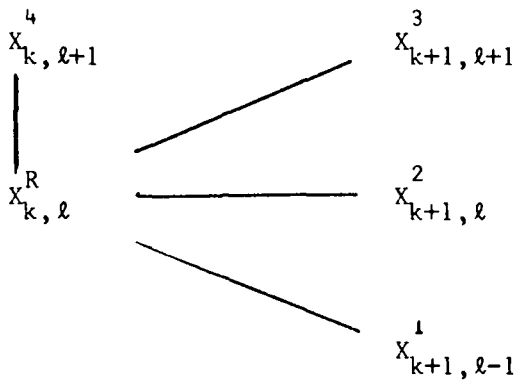

Figure 5. Neighbors of the reference pixel.

A "best link" value is computed between each of the directional probabilities of the reference pixel and all of the directional probabilities of the four neighbors. The pair giving the largest "link" value is used to update the directional probability of the reference pixel. According to the linking formulation and update, successive iterations should cause the true edges to grow as the number of iterations increases. Several methods of display were attempted but had drawbacks, since it was difficult to delineate direction on the display screen. Lott[4] settled on a display of the magnitudes of the largest probability measure of the four-component vector.

The relaxation algorithm utilizes the services of the CYBER and the STARAN, the latter doing the bulk of the computations.

Zero-Crossings - This algorithm, developed by Marr and Hildreth[5], looks for intensity changes in an image by examining the second derivative of the normal distribution. Intensity changes will occur wherever the first

---

[4]R. W. Lott, R.O. Faiss, S.G. Stadelman, STARAN Image Processing, Final Technical Report, U.S. Army Engineer Topographic Laboratories, Fort Belvoir, Va., ETL 0243, October 1980, AD-A091 928.

[5]D. Marr and E. Hildreth, "Theory of Edge Detection," AI Memo No. 518, Massachusetts Institute of Technology, Cambridge, April 1979.

Compass names indicate the gradient direction of maximum response. For example, the west mask produces a maximum output for horizontal reflectance changes from right to left. The actual direction of the line is 90° clockwise from the gradient direction. For a west gradient direction, the line direction will be to the north. See figure 4.

Each edge mask is convolved with the same neighborhood (3 by 3 in the Prewitt masks) and the response is divided by the estimates of noise of that 3 by 3 neighborhood for normalization purposes. The resultant value (one for each mask) is an estimate of the likelihood that an edge exists in that direction. In practice, only four gradient directional masks were used (NE, N, NW, and W), because a negative reflectance response indicates that the gradient direction is actually in the diametric direction; e.g., a negative response to the west mask indicates an east gradient direction. At the end of the first stage of this relaxation algorithm, therefore, there exists for each pixel a vector of four probabilities that an edge exists in the -45°, 0°, 45°, and 90° line direction.

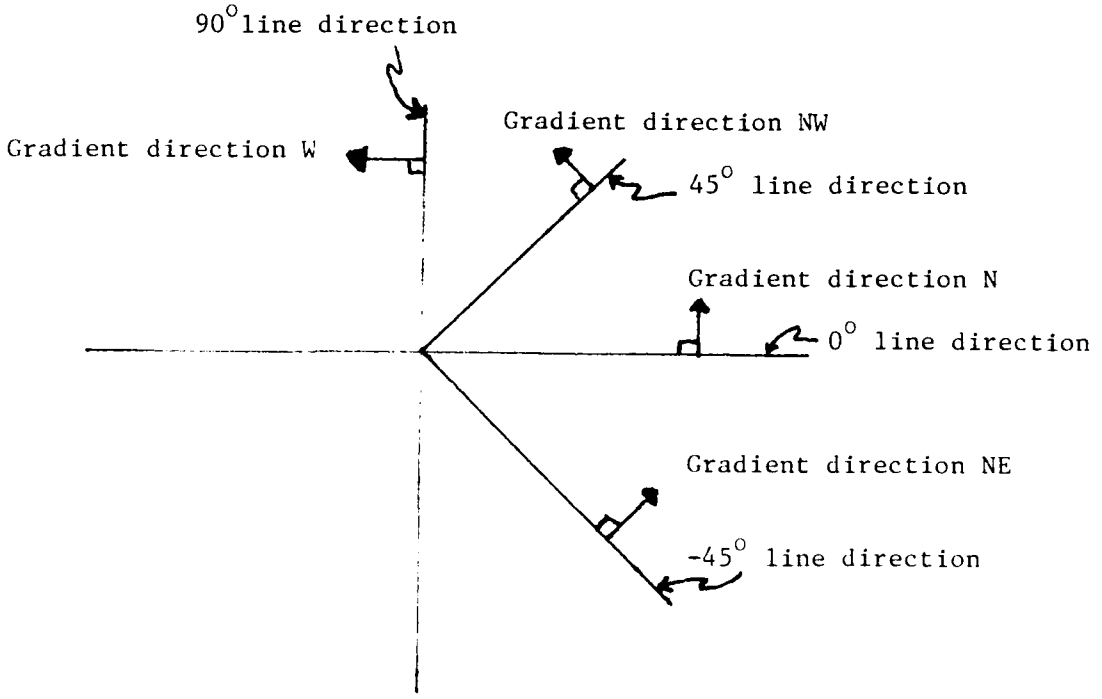

Figure 4. Relationship of line directions to gradient directions.

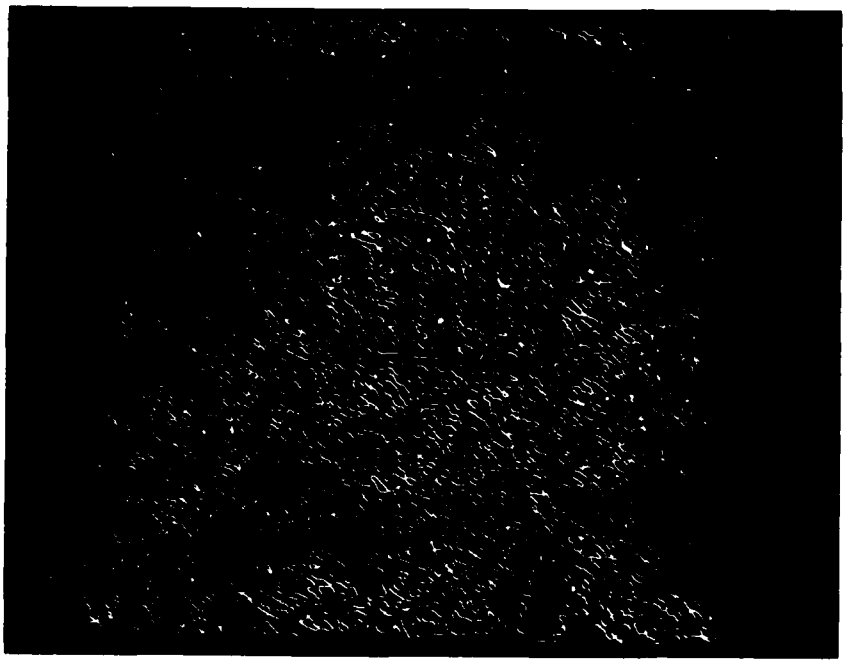

Figure 22. Zero-crossings of 27 by 27 Marr window with $\sigma = 3$ convolved with CBP54A.

Marr Zero-Crossings - The Marr algorithm produces impressive visual results, but it is difficult to produce an "edge/no edge" map from it. If one desires a "quick and dirty" representation of an edge map, then a single Marr zero-crossings representation in conjunction with the RASTER PM will produce acceptable results. The RASTER PM, when finished, will be capable of eliminating clutter, filling closed areas, and thinning to center lines, thus creating some semblance of an edge map.

The smaller windows that are produced from the smaller sigma values generate noisier images than do the larger windows, but their results present a more definitive representation of the edges, particularly evidenced in the samples depicted in appendix A. When two or more windows with differing sigmas produce coincident edges, those edges most likely are due to the presence of intensity changes in the image. Thus, one can produce an "edge/no edge" map by comparing several windows, but the results will not be as complete as when deriving the edge map from the convolved results of a small window.

CONCLUSIONS

1. The nonlinear method of edge detection generates a good visual representation. It is difficult to use the results, though, in combination with other feature extractors, as pertinent data is lost converting the results to a useable format.

2. The images produced from the directional edge-relaxation method of detection were inferior to those produced by the Sobel method. Edges were not as well defined and the images were of poorer quality.

3. The zero-crossings operator produces a unique representation of edges, but its utility will depend upon developing an effective cleanup PM like RASTER.

4. Use of a stereo image is valuable in picking up additional information because of the different perspective presented by the stereomate. However, in order to transfer newly identified data from one image to its stereomate, it is necessary to register the two images in order to extract and/or overlay the additional information.

APPENDIX A

RESULTS OF VARIOUS MARR WINDOW CONVOLUTIONS

Background - The Marr algorithm was originally tested at ETL on a drainage pattern subset of a Phoenix model and the results were impressive. However, the Marr windows produced by the larger sigma values ($\sigma \geq 3$) were quite large and required an excessive amount of computer time to perform the convolution of the Marr window with the image. In an effort to decrease the turnaround time, it was decided to perform the convolutions in frequency space instead of in the spatial domain as was originally done. This step successfully reduced computation time from 30 minutes to 70-90 seconds for larger sized filters. It was also decided to examine the filter sizes to determine if the pertinent information could be contained in a reduced filter size, and what filter sizes are appropriate to the various sigma values. This appendix presents the results of the convolutions on the Phoenix model with varying Marr filters.

Theoretically, the sum of the filter values should be equal to zero. But according to the table in figure A1, for a sigma value of 3, any of the filters from size 23 by 23 up to size 33 by 33 could qualify, depending on the accuracy required. From the table labeled figure A2, it would appear that the outer five rows would contribute insignificantly to the results because their values are relatively small. The sum of the filter "weights" for this filter is equal to .0001.

Results - It can be seen from the table in figure A1 that by extracting a smaller window, e.g., a 19 by 19, from the center of the entire Marr filter, the convoluted result becomes more positive, thus biasing the results to some extent. This bias is due to the fact that the eliminated filter values are all negative. The effect, though, can be an advantage as can be seen in figures A4 through A17, which are the results of convolutions of Marr windows with the drainage pattern subset of our PHOENIX model, figure A3.

σ	WINDOW	FILTER SUM
1	5	.934
1	7	.051
1	9	.001
2	11	9.524
2	13	2.445
2	15	.473
2	17	.070
2	21	.000
3	15	86.799
3	17	40.417
3	19	16.513
3	21	5.953
3	23	1.900
3	25	.538
3	27	.135
3	29	.030
3	31	.006
3	33	.001
4	15	778.852
4	25	59.596
4	27	28.470
4	29	12.695
4	33	2.061
5	15	2649.210
5	31	156.960
5	41	5.618
5	49	.181
8	49	1148.757

Figure A1. Sum of filter values for various Marr windows.

	1	2	3	4	5	6	7	8	9	10	11	12	13	14	15	16	17
1	-.00	-.00	-.00	-.00	-.00	-.00	-.00	-.00	-.00	-.00	-.00	-.00	-.00	-.00	-.00	-.00	-.00
2	-.00	-.00	-.00	-.00	-.00	-.00	-.00	-.00	-.00	-.00	-.00	-.00	-.00	-.00	-.00	-.00	-.00
3	-.00	-.00	-.00	-.00	-.00	-.00	-.00	-.00	-.00	-.00	-.00	-.00	-.00	-.00	-.00	-.00	-.00
4	-.00	-.00	-.00	-.00	-.00	-.00	-.00	-.00	-.00	-.00	-.00	-.00	-.01	-.01	-.01	-.01	-.01
5	-.00	-.00	-.00	-.00	-.00	-.00	-.00	-.00	-.00	-.00	-.01	-.01	-.02	-.03	-.03	-.04	-.04
6	-.00	-.00	-.00	-.00	-.00	-.00	-.00	-.00	-.01	-.01	-.02	-.04	-.06	-.08	-.10	-.12	-.12
7	-.00	-.00	-.00	-.00	-.00	-.00	-.00	-.01	-.02	-.03	-.06	-.10	-.16	-.21	-.27	-.30	-.32
8	-.00	-.00	-.00	-.00	-.00	-.00	-.01	-.02	-.04	-.08	-.15	-.24	-.36	-.49	-.60	-.67	-.70
9	-.00	-.00	-.00	-.00	-.00	-.01	-.02	-.04	-.09	-.18	-.32	-.51	-.73	-.95	-1.14	-1.27	-1.31
10	-.00	-.00	-.00	-.00	-.00	-.01	-.03	-.08	-.18	-.35	-.60	-.92	-1.27	-1.59	-1.84	-1.99	-2.04
11	-.00	-.00	-.00	-.00	-.01	-.02	-.06	-.15	-.32	-.60	-.99	-1.45	-1.89	-2.22	-2.38	-2.43	-2.44
12	-.00	-.00	-.00	-.00	-.01	-.04	-.10	-.24	-.51	-.92	-1.45	-1.99	-2.36	-2.42	-2.20	-1.89	-1.75
13	-.00	-.00	-.00	-.01	-.02	-.06	-.16	-.36	-.73	-1.27	-1.89	-2.36	-2.37	-1.75	-.66	.39	.82
14	-.00	-.00	-.00	-.01	-.03	-.08	-.21	-.49	-.95	-1.59	-2.22	-2.42	-1.75	0.00	2.43	4.59	5.46
15	-.00	-.00	-.00	-.01	-.03	-.10	-.27	-.60	-1.14	-1.84	-2.38	-2.20	-.66	2.43	6.41	9.85	11.21
16	-.00	-.00	-.00	-.01	-.04	-.12	-.30	-.67	-1.27	-1.99	-2.43	-1.89	.39	4.59	9.85	14.32	16.08
17	-.00	-.00	-.00	-.01	-.04	-.12	-.32	-.70	-1.31	-2.04	-2.44	-1.75	.82	5.46	11.21	16.08	18.00

Figure A2. Upper left quadrant of Marr 33 by 33 window for $\sigma = 3$.

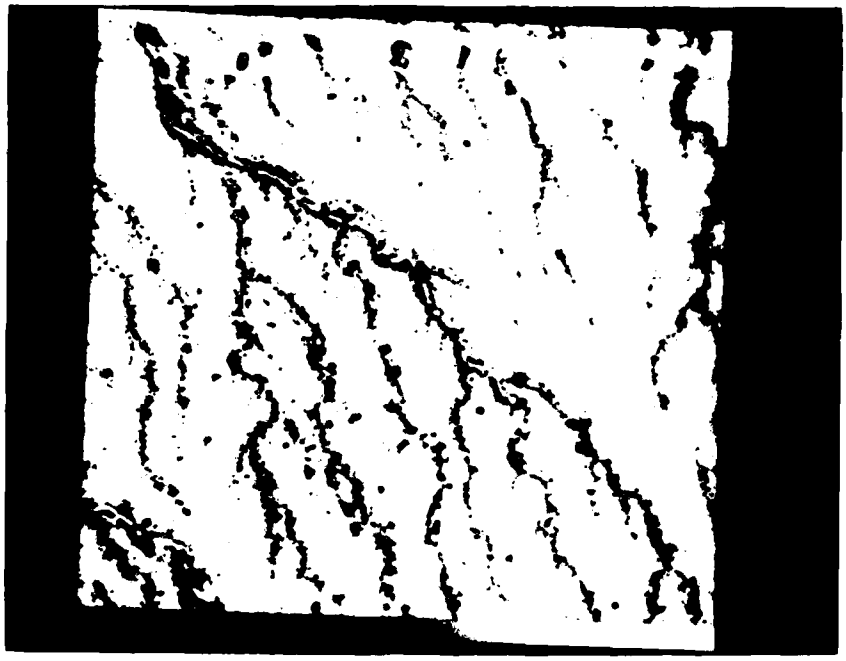

Figure A3. TE512 subset of PHOENIX model REC01.

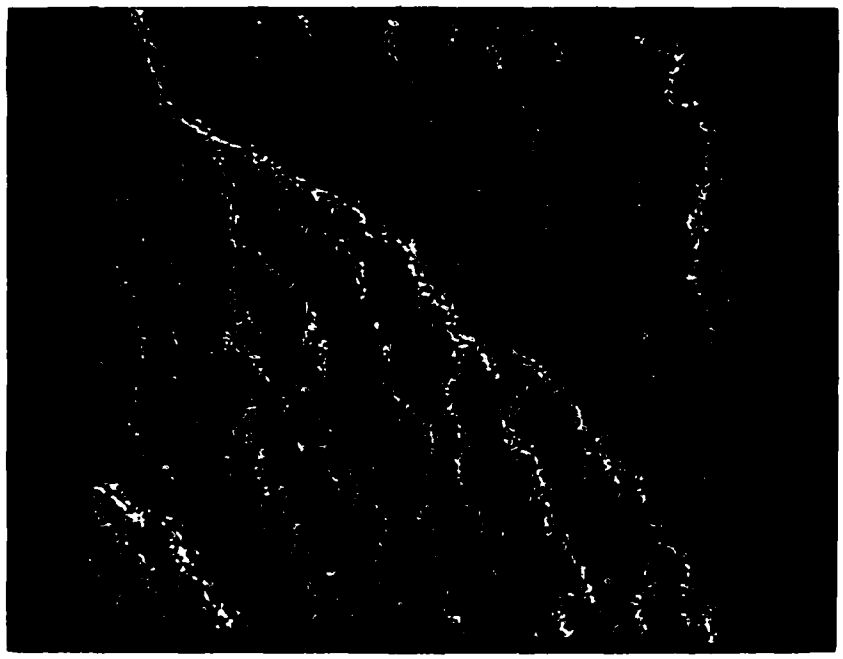

Figure A4. Zero-crossing of 5 by 5 Marr window, $\sigma = 1$.

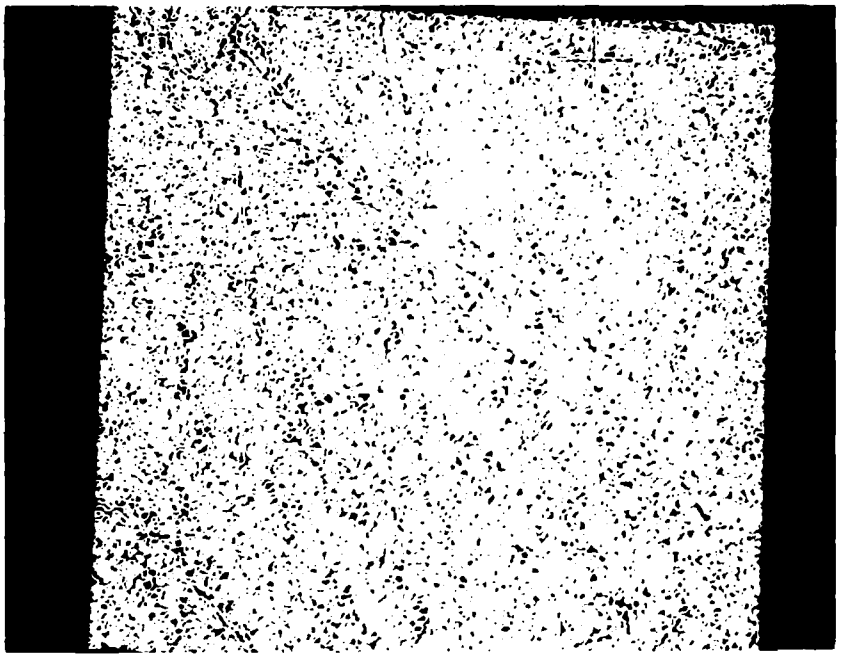

Figure A5. Zero-crossing of 7 by 7 Marr window, $\sigma = 1$.

Figure A6. Zero-crossing of 11 by 11 Marr window, $\sigma = 2$.

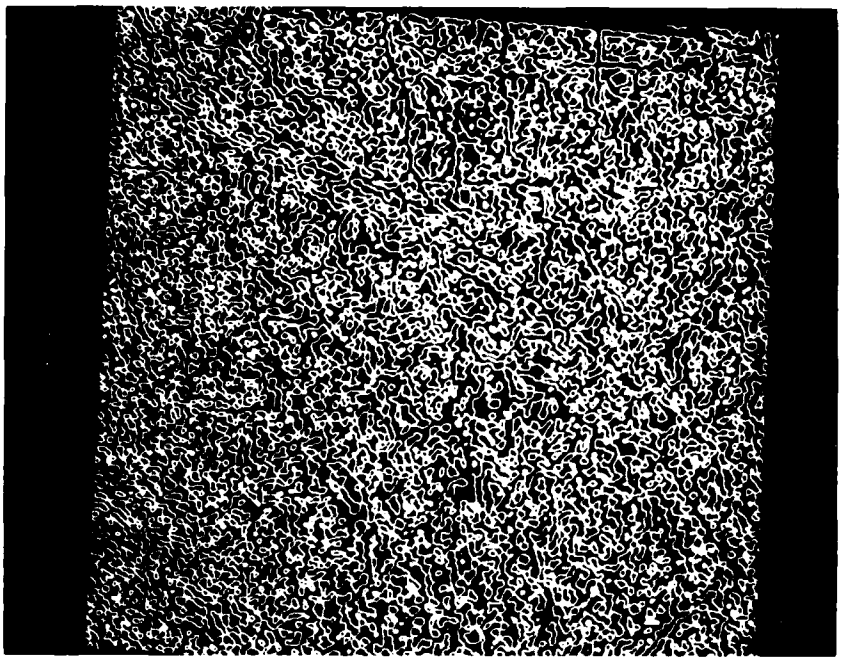

Figure A7. Zero-crossing of 15 by 15 Marr window, $\sigma = 2$.

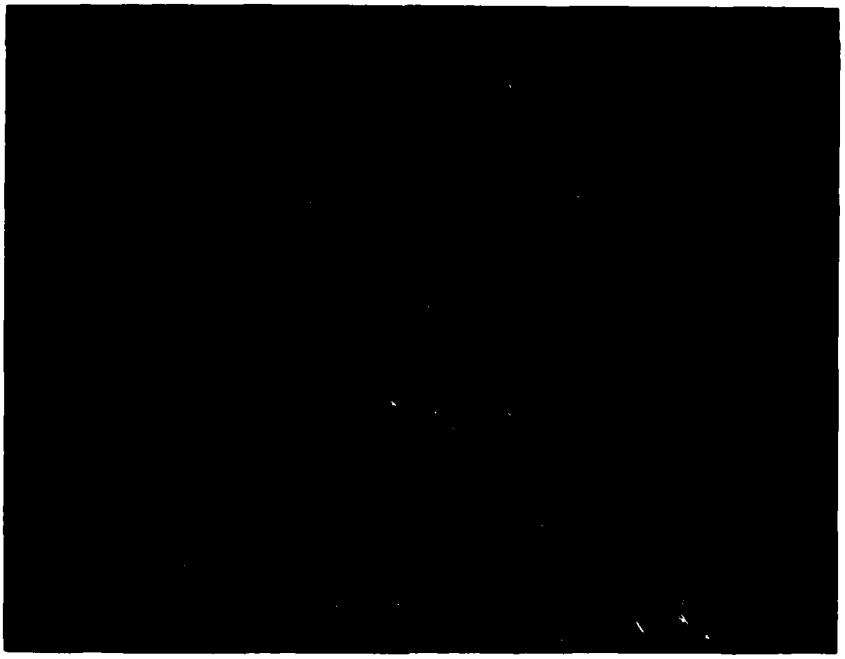

Figure A8. Zero-crossing of 15 by 15 Marr window, $\sigma = 3$.

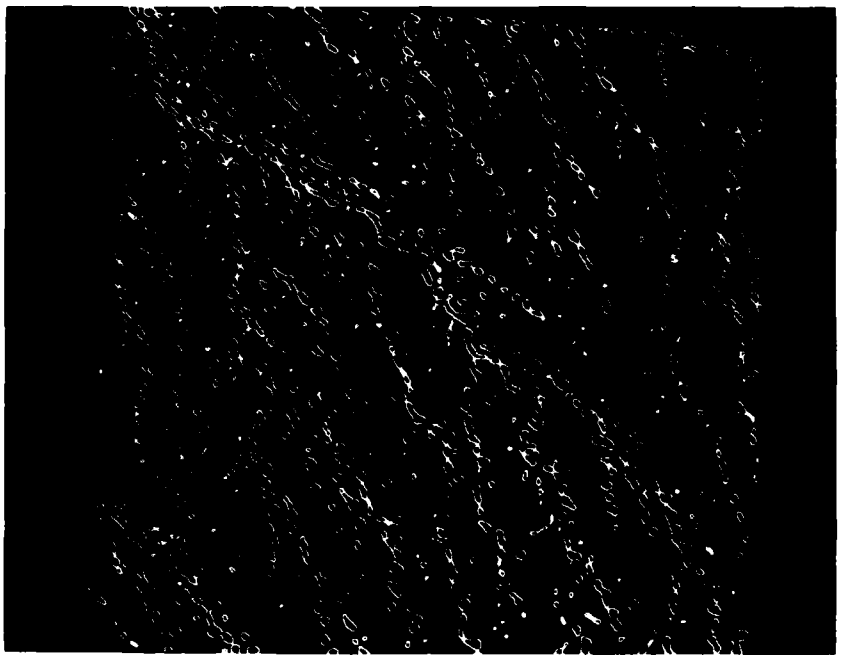

Figure A9. Zero-crossing of 17 by 17 Marr window, $\sigma = 3$.

Figure A10. Zero-crossing of 19 by 19 Marr window, $\sigma = 3$.

Figure A11. Zero-crossing of 21 by 21 Marr window, $\sigma = 3$.

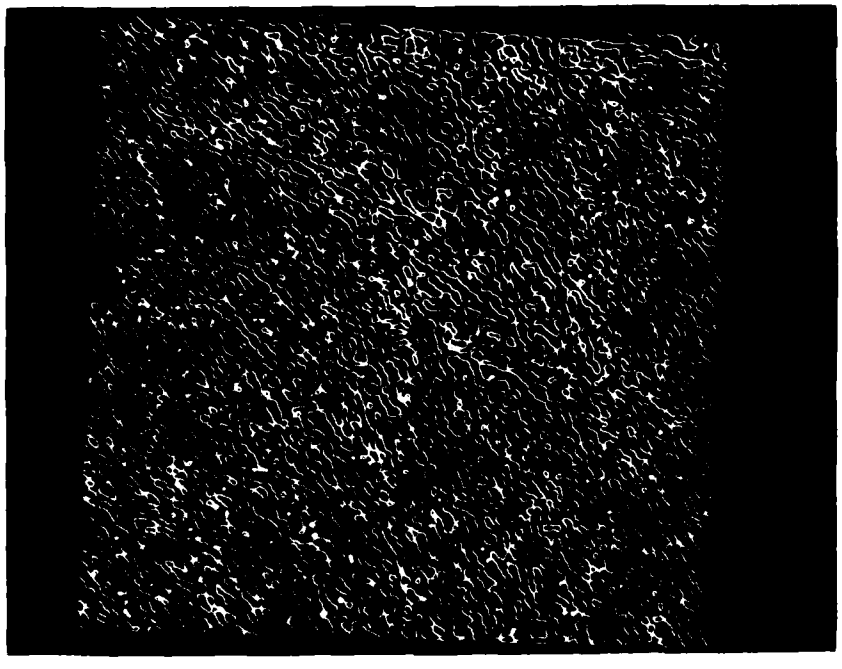

Figure A12. Zero-crossing of 23 by 23 Marr window, $\sigma = 3$.

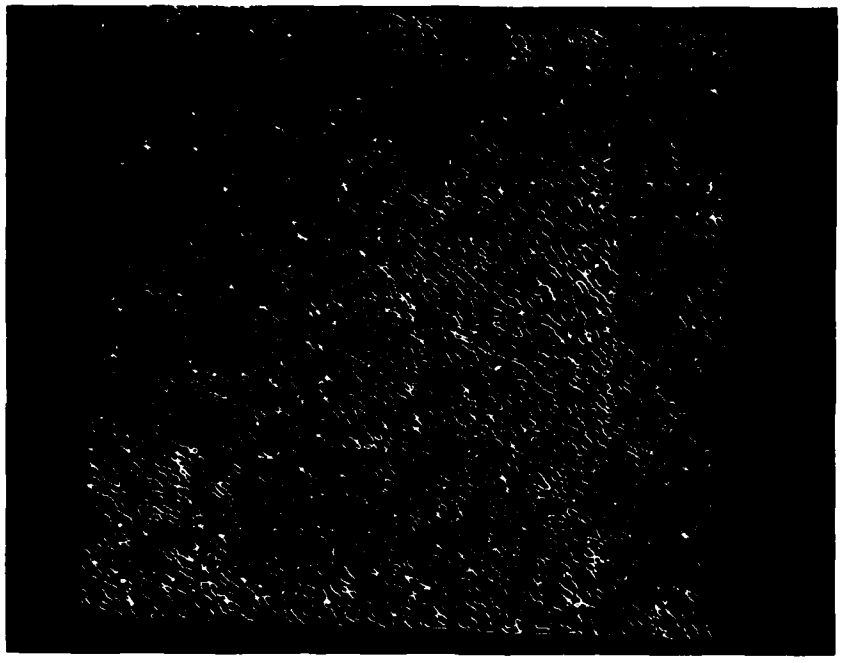

Figure A13. Zero-crossing of 25 by 25 Marr window, $\sigma = 3$.

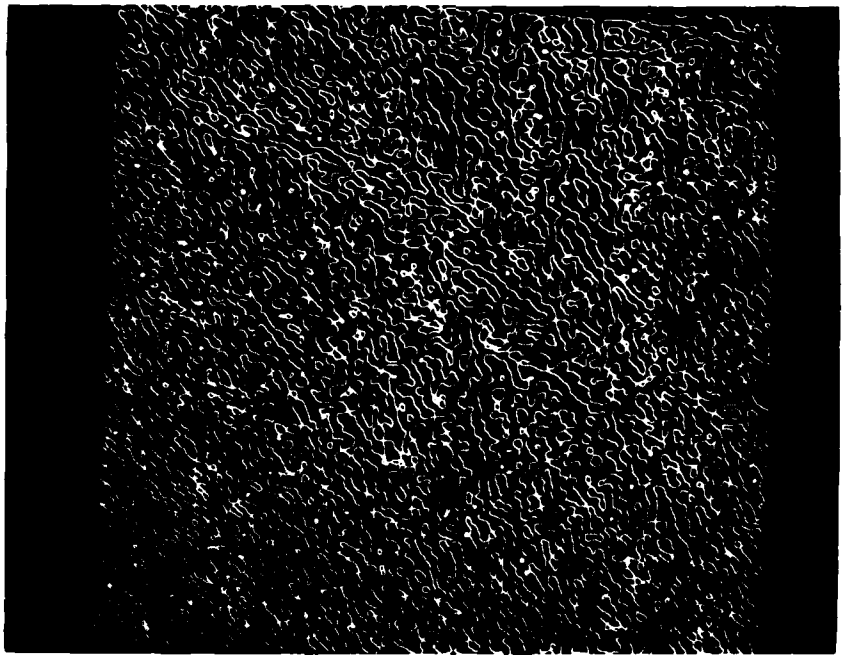

Figure A14. Zero-crossing of 27 by 27 Marr window, $\sigma = 3$.

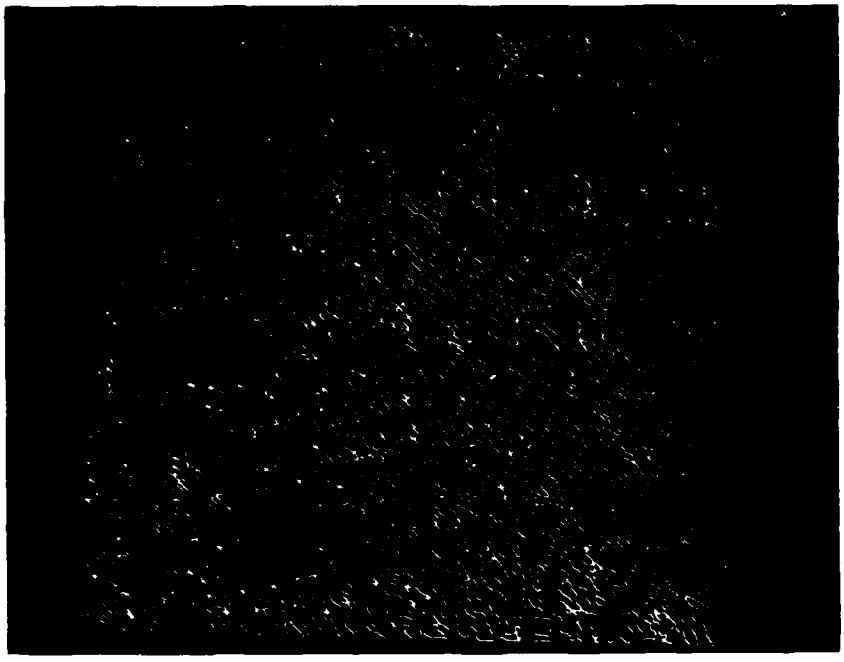

Figure A15. Zero-crossing of 31 by 31 Marr window, $\sigma = 3$.

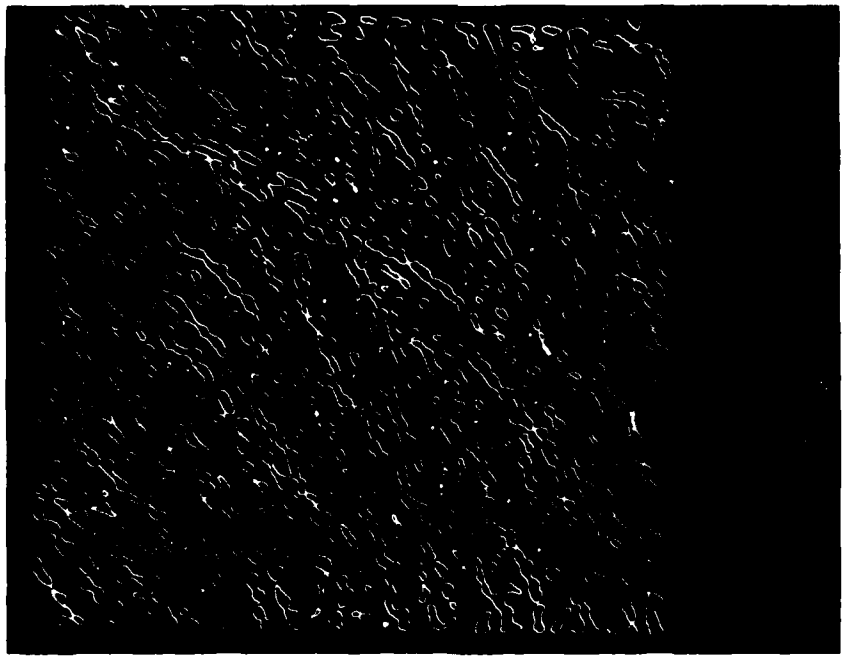

Figure A16. Zero-crossing of 25 by 25 Marr window, $\sigma = 4$.

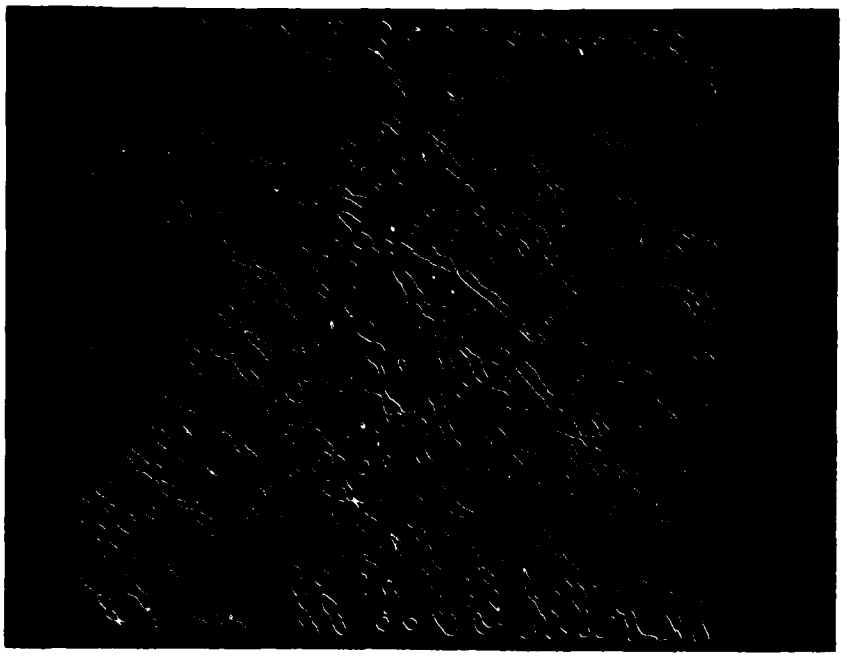

Figure A17. Zero-crossing of 31 by 31 Marr window, $\sigma = 5$.

After looking at the results in figures A5, A7, and A12 through A15, one sees that little can be done with extracting edges even by means of clutter removal. Please note that for these filters the sum of the weights approaches zero. In the series of pictures for $\sigma = 3$, a better choice for a representative pattern of edges would be figure A10, where a cleanup process might be more manageable. Note that for figure A10, the sum of the filter values is 16.513.

Additional exercises were undertaken to force the sum of the filter values to be zero when the filter was large and when a smaller filter with which to work was desired. Two options were tried: (1) by subtracting from each value of the filter an average correction based on the sum of the filter weights, and (2) by decreasing only the positive values of the original filter. Neither option was acceptable, as the resulting zero-crossings images were just as "busy" as the original and did not suit our purposes for extracting an edge. Another exercise involved a thresholding technique. The floating point array that is created by the convolution was histogrammed in order to get some idea of the distribution of the values. From this histogram, a threshold range could be selected to test the existence of a zero-crossing in order to make the procedure less sensitive to noise in the image. It was found, however, that thresholding destroyed the well-defined closed ellipses, rendering the image useless for some rastering techniques.

☆ U.S. GOVERNMENT PRINTING OFFICE : 1985 O - 461-063 (26511)

END

FILMED

8-85

DTIC